Open access • Journal Article • DOI:10.1111/J.1365-246X.2006.03140.X

Rheological characterization of a sedimentary formation from a stress profile inversion — Source link

Yann Gunzburger, Yann Gunzburger, François Cornet

Institutions: IPG Photonics, Australian National Drag Racing Association

Published on: 01 Jan 2007 - Geophysical Journal International (Oxford University Press)

Topics: Stress field, Pressure solution and Sedimentary rock

Rheological characterization of a sedimentary formation from a stress profile inversion

Yann Gunzburger, François Cornet

Geophys. J. Int. (2007) **168,** 402–418 doi: 10.1111/j.1365-246X.2006.03140.x

Rheological characterization of a sedimentary formation from a stress profile inversion

Y. Gunzburger[1,2] and F. H. Cornet[1]

[1] *Institut de Physique du Globe, Département de Sismologie, Case* 89, 4 *place Jussieu,* 75252 *Paris cédex* 5, *France. E-mail: gunzburg@ipgp.jussieu.fr*
[2] *ANDRA, Laboratoire de Recherche Souterrain de Meuse/Haute-Marne, RD* 960, BP 9, 55290 *Bure, France*

Accepted 2006 July 11. Received 2006 July 7; in original form 2006 January 23

SUMMARY

Detailed stress measurements have been carried out within a sedimentary sequence composed of a hard-clay formation laying horizontally between two limestone units, in the eastern Paris basin (France). Orientations of the minor and major horizontal principal stresses are found to be in good agreement with the direction of major shortening that prevailed during the last tectonic stage. However, their magnitudes exhibit an intriguing evolution with depth. While the magnitude of the maximum horizontal stress slowly but regularly increases with depth, the magnitude of the minimum horizontal one is larger in the hard-clay formation than in the surrounding limestone units, contrary to expectation from simple elastic considerations. An analytical calculation demonstrates that the genesis of the current stress state may be reproduced by taking into account horizontal strains in two different directions and simulating erosion of part of the overburden with a viscoelastic model for the hard clay and an elastic behaviour for the limestone. However, the elastic constants that are derived for the limestone in order to fit the measured stress field correspond to a material that is more deformable and has a lower Poisson's ratio than predicted by laboratory tests. This discrepancy may be explained by a slow, long-term, deformation process in the limestone, possibly associated with pressure solution.

Key words: inverse problem, rheology, scale effect, sedimentary basin, stress distribution, viscoelasticity.

1 INTRODUCTION

The regional stress field that exists today in a given rock mass depends on the present-day loading conditions (gravity and boundary conditions) but also, generally, on the loading history through the rheology of the rock mass. The objective of this paper is to discuss the problem of near-surface stress genesis and to propose a method based on the analysis of vertical stress profiles to identify key rheological parameters that characterize the behaviour of a rock mass at geological timescale, which are currently out of reach to all laboratory and *in situ* tests. The method is applied to the Jurassic rocks of the eastern Paris basin (France), in an area where the loading history (i.e. the past geological events) and the resulting structures are particularly simple.

First the geological setting of the site under study is briefly described together with the results of the very comprehensive stress measurements campaigns that have been conducted. Then limitations of an elastic geomechanical model for interpreting the observed stress field are outlined and a viscoelastic model is introduced, whose parameters can be estimated from stress profile inversion. Finally a discussion shows how the deformation history of the stiffest rocks (limestone) controls the present-day stress field in the softer clayish formation, a feature that is tentatively related to pressure-solution effects in the limestone.

2 GEOLOGICAL SETTING AND GEOMECHANICAL DATA

The site under study is that of the Underground Research Laboratory (URL) currently developed by ANDRA (the French national radioactive waste management agency) for investigating the feasibility of a safe long-term nuclear waste underground repository (ANDRA 2005). It is located near the small village of Bure, some 250 km east of Paris (Fig. 1a). The target material is a hard-clay unit encountered within the 420 to 550 m depth interval (the so-called '*Bure argillite*' formation) and corresponds to a mixture of 45–50 per cent micas clays, 25–30 per cent

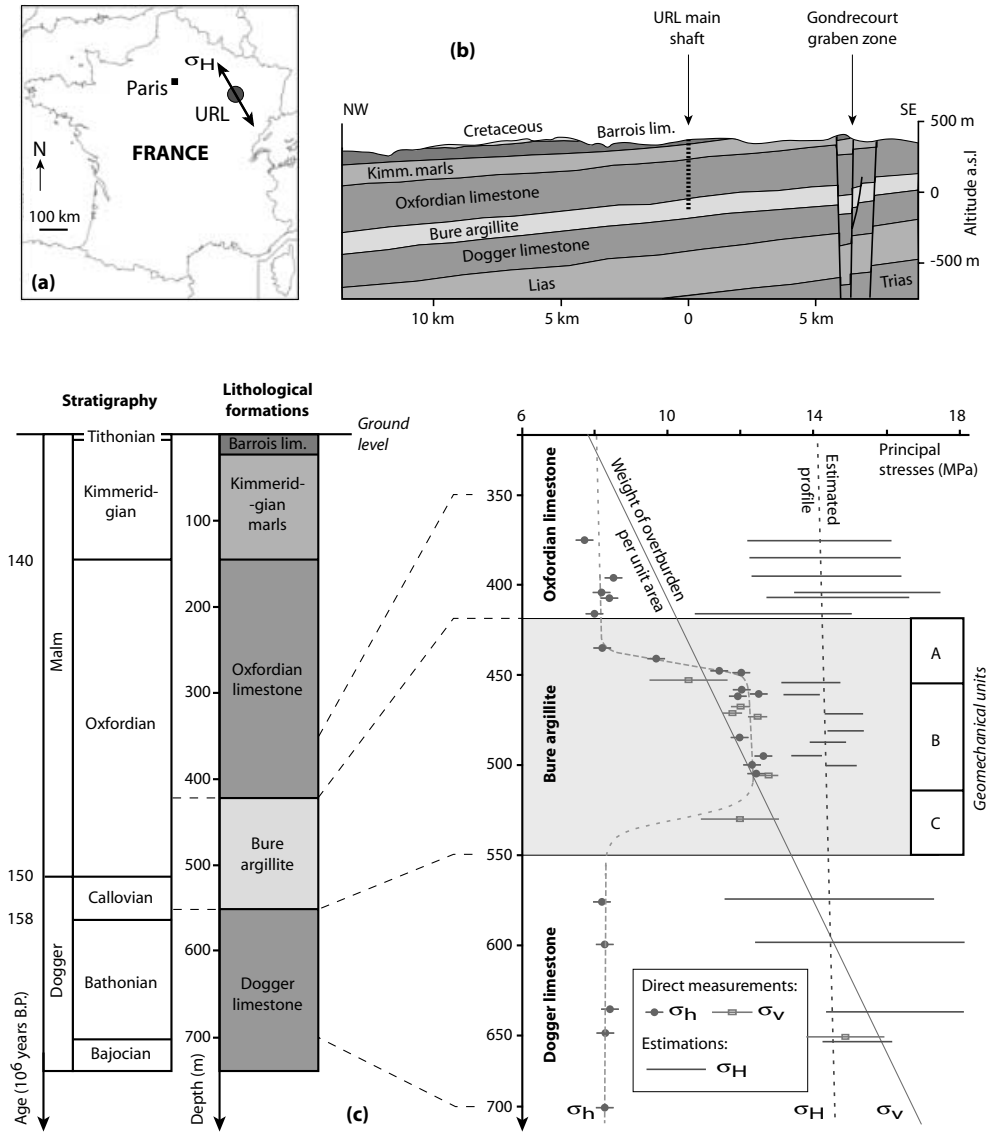

Figure 1. Geological setting and present stress state in the vicinity of the Bure URL. (a) Location of the URL in eastern France and orientation of the major horizontal principal stress. (b) Cross-section showing the simplicity of the geological structures. Note that horizontal and vertical length scales are different. (c) Vertical profile of principal stress magnitudes derived from stress measurement campaigns (Wileveau *et al.* 2006). Estimations of σ_H also take into account systematic analysis of borehole breakouts and shaft convergence monitoring.

calcite and 20 per cent quartz. It is dated from the Callovo–Oxfordian (about 150 Myr BP) and is lying above the '*Dogger limestone*' and below the '*Oxfordian limestone*' formations (Fig. 1b), both of which are stiffer, carbonate-rich, units.

The last tectonic episode that affected this region was characterized by a major horizontal shortening direction oriented NNW–SSE (André 2003). It is related to the Alpine orogenic phase, whose maximal intensity was reached during Miocene (24 to 5 Myr BP). Since that time, no significant tectonic event has occurred and the geological evolution is governed by progressive surface erosion. Topography is presently very smooth (it probably ever was) and the bedding is quite horizontal, with a very low dipping angle toward the NW (about 1.5°). No fault has been identified close to the URL site, as concluded from the very comprehensive geological survey and seismic imaging program that has been conducted for its reconnaissance.

A great amount of laboratory tests have been carried out on samples from various depths, providing a very satisfactory overview of the rheological properties of the rock mass at a timescale of several minutes to hours (Table 1).

In addition, ANDRA has carried out a very extensive stress evaluation program through classical hydraulic fracturing tests (Haimson 1993), hydraulic testing on pre-existing fractures (so-called 'HTPF method', Cornet 1993), sleeve reopening tests (Stephansson 1983), shaft convergence monitoring and systematic analyses of borehole breakouts (Zoback *et al.* 2003). This has resulted in a rather continuous vertical stress profile through the limestone–argillite–limestone sequence (Wileveau *et al.* 2006), with an excellent resolution on all the components of the stress tensor throughout the domain of investigation. Hydraulic fractures and borehole breakouts constrain principal directions. Hydraulic fracturing tests constrain the minimum principal stress magnitude. HTPF and sleeve reopening yield the vertical

Table 1. Average physical and mechanical properties of the different lithological units derived from classical laboratory tests (*) and from borehole sonic logging (**). Static and dynamic parameters are in good agreement in the case of the limestone formations, whereas the average static Young's modulus of the argillite is four to five times lower than the dynamic one. Such a contrast may be attributed to non-elastic deformation during laboratory tests, possibly associated with short-term creep.

		Bulk ($g\,cm^{-3}$) density	Static Young's modulus (GPa)*	Static Poisson's ratio*	UCS (MPa)*	UTS (MPa)*	Dynamic Young's modulus (GPa)**	Dynamic Poisson's ratio**
Oxfordian limestone		2,50 ± 0,12	15–40	?	25–75	?	38 ± 10	0.3 ± 0.02
Bure argillite	A unit	2,44 ± 0,08	5,4 ± 1,5	0,3 ± 0,05	29 ± 12	2,7 ± 1,5	21 ± 4	0.2 ± 0.1
	B - C units		4,0 ± 1,5		21 ± 7			
Dogger limestone		2,63 ± 0,05	38 ± 15	0,23 ± 0,05	53–120	2,4–8,3	46 ± 3	0.3 ± 0.01

component, while a combination of sleeve fracturing and sleeve reopening together with borehole breakouts, shaft convergence monitoring and hydraulic fracturing analysis constrain efficiently the maximum horizontal principal stress magnitude.

The vertical component of the stress tensor (σ_v) is principal and almost equal to the weight of overburden per unit area (Fig. 1c). The maximum principal horizontal stress (σ_H) is oriented N150°E ± 5° (Fig. 1a), which is in good agreement with the regional stress pattern (Cornet & Burlet 1992; Müller *et al.* 1992; Röckel & Lempp 2003, World stress map) and is close to the average major tectonic shortening direction that prevailed during the last (Alpine) orogeny. Despite some uncertainties on its exact value, σ_H is found to increase continuously with depth through the whole limestone–argillite–limestone sequence (Fig. 1c) while the minor horizontal stress (σ_h) exhibits a bed-to-bed step variation with depth. In particular, σ_h is larger in the central part of the argillite formation than in the surrounding, stiffer, limestone units.

Such lithology-correlated horizontal stress contrasts have already been documented in other horizontally layered rock masses (e.g. Evans *et al.* 1989; Warpinski & Teufel 1989, 1991; Cornet & Burlet 1992) and various interpretations have been proposed. One of them is that they result from contrasts in elastic properties (first and third references) but this involves simultaneous increase (or decrease) in σ_h and σ_H with depth, which have not been observed in our case. It has also been suggested, on a qualitative basis only, that the stress contrasts might result from stress relaxation within the clay-rich rocks (second reference). In our example, if we assume that the 'jump' in σ_h is associated with the viscous behaviour of the argillite, it is not obvious why the magnitude of σ_H does not show any drop within the corresponding depth interval. Moreover, one might expect the two horizontal stresses to be equal to the vertical one within the argillite formation, which is not the case. Thus, the validity of the proposed interpretations has to be analysed more quantitatively.

In the next section we evaluate the stress profile that would have been anticipated from a simple elastic equilibrium after the Alpine orogeny has ceased being active and erosion has occurred.

3 THE STRESS STATE IN AN INFINITE PLATE UNDER GRAVITY

3.1 Static equilibrium under gravity

In a situation of static equilibrium as that of the studied area, the stress tensor $\overline{\overline{\sigma}}$ is linked to the gravitational acceleration $\overrightarrow{g}$ and the bulk density ρ by:

$$\mathrm{div}\,\overline{\overline{\sigma}} + \rho\,\overrightarrow{g} = \overrightarrow{0}\,. \tag{1}$$

This relation is not sufficient to determine completely the stress state and additional relations have to be found in order to get a mathematically fully solvable problem. In particular, the stress field must also satisfy appropriate boundary conditions as well as the rheological law of the considered material. Thus, it generally depends on the geological history.

For example, calculating the gravity-induced stress state in a homogeneous, linearly elastic half-space with horizontal surface is a well-known problem (Jaeger & Cook 1976) in which, due to equilibrium law, one principal stress direction is vertical with a magnitude σ_v equal to the weight of overburden per unit area. The two other stresses are horizontal and have the same magnitude, but they are not determined if no supplementary assumption is made. Even if it is not the only possible solution, it is often assumed that:

$$\sigma_H = \sigma_h = \alpha\sigma_v = \alpha\rho g z, \tag{2}$$

where z stands for depth below ground surface. α is a coefficient that depends on the local conditions (type of rocks, geological history, etc.) the value and meaning of which have been considerably discussed.

In absence of additional information, it is generally assumed that α is equal to 1 (hypothesis of total stress relief proposed by the Swiss geologist Heim in 1878) or to $\frac{\nu}{1-\nu}$ (denoted κ from now on) with ν being Poisson's ratio (hypothesis of vanishing lateral displacements, Amadei & Stephansson 1997, chap. 2). These assumptions rely on considerable simplification and none of them directly applies to our case since at any given depth, the ratios σ_H/σ_v and σ_h/σ_v are not equal. However, the second hypothesis ($\alpha = \kappa$) may explain part of the present stress profile because the stress gradients are then controlled by Poisson's ratio. Actually, as shown by Amadei *et al.* (1988), eq. (2) may be extended to the case of a horizontally layered rock mass consisting of strata with different mechanical properties. In such a case, σ_v must be

continuous at layer interfaces (it remains equal to the weight of overburden per unit area) while σ_h and σ_H may not be continuous. In particular jumps in σ_h and σ_H may occur from one layer to another in relation with variations in Poisson's ratio: σ_h/σ_v and σ_H/σ_v will be higher in rocks with higher Poisson's ratio and *vice versa*.

Independently, in a transversally isotropic stratum with vertical axis of symmetry, the horizontal stresses expression becomes (Amadei *et al.* 1988):

$$\sigma_H = \sigma_h = \frac{E_{/\!/}}{E_\perp}\frac{\nu_\perp}{1-\nu_{/\!/}}\sigma_v, \tag{3}$$

where the subscripts $/\!/$ and $\perp$, respectively, refer to the elastic constants in the horizontal isotropic plane and in the vertical direction. As a consequence, the ratio of horizontal to vertical stress components also increases with the degree of anisotropy of the stratum (increasing value for $E_{/\!/}/E_\perp$ in particular). From laboratory tests, *Bure argillite* is known to exhibit higher Poisson's ratio than does the limestone (Table 1) and to be slightly anisotropic ($E_{/\!/}/E_\perp = 1.5$, Zhang & Rothfuchs 2004). These results may explain that σ_h/σ_v exhibits a higher value in the argillite formation than in the surrounding limestone rocks. However, they imply the same conclusion for σ_H/σ_v, which is not in agreement with the measurements. For this reason, we will not consider anisotropy anymore. This feature could be added later in a more sophisticated model, if necessary.

The discrepancy between predictions and measurements is due to the over-simplistic assumptions we made. Indeed the state of stress cannot be deduced from the present geometry only, as if gravity was 'turned on' suddenly with the stresses changing at once from zero to their present value. In the next section, we examine the consequences of both erosion of part of the overburden and of horizontal strains that account for far-field loading, possibly of tectonic origin.

3.2 Elastic effects of horizontal strains and erosion

Using the analytical solution proposed by McGarr (1988) and Goodman (1989), one may calculate the stress change that occurs after removal of a layer of overburden with thickness Δz. Let us assume that the stress state before erosion, at the initial depth $z + \Delta z$, is given by:

$$\begin{cases} \sigma_v = \rho g(z+\Delta z) \\ \sigma_H = \sigma_h = \alpha_i \rho g(z+\Delta z) \end{cases}. \tag{4}$$

Because α may vary form one layer to another, the subscript i denotes the material under consideration. If no horizontal displacement is allowed, the stress state after erosion (at the final depth z) is:

$$\begin{cases} \sigma_v = \rho g z \\ \sigma_H = \sigma_h = \alpha_i \rho g(z+\Delta z) - \frac{\nu_i}{1-\nu_i}\rho g \Delta z = \alpha_i \rho g z + (\alpha_i - \kappa_i)\rho g \Delta z \end{cases}. \tag{5}$$

If $\alpha_i \neq \kappa_i$, this results in non-zero horizontal stresses at ground surface.

However, the difference we observed between the two horizontal stresses cannot be accounted for by the hypothesis of zero lateral displacement. For this purpose we evaluate hereafter the effect of applying strains ε_h and ε_H (oriented parallel to the directions of σ_h and σ_H) to simulate past horizontal strains. According to Savage *et al.* (1992), the stress changes induced by these strains are:

$$\begin{cases} \Delta\sigma_v = 0 \\ \Delta\sigma_H = \frac{E_i}{1-\nu_i^2}(\varepsilon_H + \nu_i \varepsilon_h) \\ \Delta\sigma_h = \frac{E_i}{1-\nu_i^2}(\nu_i \varepsilon_H + \varepsilon_h) \end{cases}. \tag{6}$$

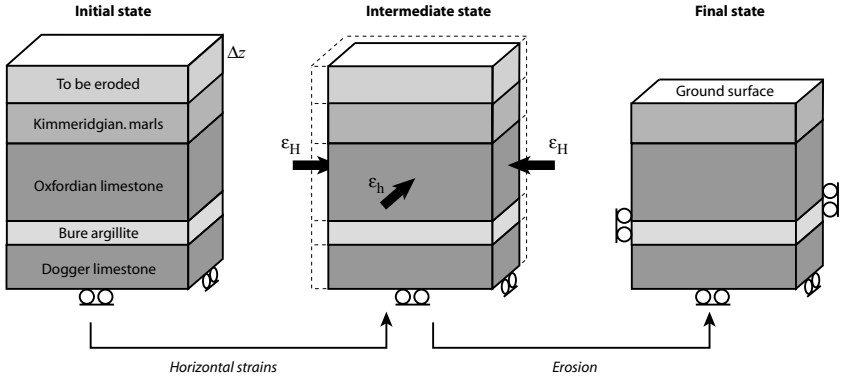

Figure 2. Geometrical model used for analytical calculations. At the first step, homogeneous horizontal strains are applied in both H and h directions. At the second step, a slice of overburden is eroded while further horizontal deformations are prevented.

Thus, cumulating the effects of horizontal strains and erosion (Fig. 2), we obtain:

$$\begin{cases} \sigma_v = \rho g z \\ \sigma_H = \alpha_i \rho g z + (\alpha_i - \kappa_i)\rho g \Delta z + \frac{E_i}{1-\nu_i^2}(\varepsilon_H + \nu_i \varepsilon_h) = \alpha_i \rho g z + \sigma_{H,i}^{z=0} \\ \sigma_h = \alpha_i \rho g z + (\alpha_i - \kappa_i)\rho g \Delta z + \frac{E_i}{1-\nu_i^2}(\nu_i \varepsilon_H + \varepsilon_h) = \alpha_i \rho g z + \sigma_{h,i}^{z=0} \end{cases} . \tag{7}$$

These expressions may be generalized to the case of a rock mass with non-uniform density by replacing terms $\rho g z$ and $\rho g \Delta z$ by the weights of the present overburden and that of the eroded overburden per unit area. However, this it is not necessary here since densities are close to each other (Table 1).

Other possible stress-modifying processes that are not taken into account in this paper may be invoked in future studies, such as changes in pore pressure (Evans *et al.* 1989) and changes in temperature. In particular, Turcotte & Schubert (2002, pp. 171–174) consider the effects of geotherm re-equilibration after erosion. If β represents the geothermal gradient (K/m) and λ_T the linear thermal expansion coefficient (K^{-1}), they calculate the thermally induced change in horizontal stresses associated with erosion:

$$(\Delta\sigma_H)_T = (\Delta\sigma_h)_T = -\frac{E\lambda_T\beta}{1-\nu}\Delta z. \tag{8}$$

Thus, thermal effects may shift both horizontal strains by a constant value, but affect neither their vertical gradients nor the horizontal differential stress $\sigma_H - \sigma_h$.

3.3 Fitting the model with the measured stress profile

In the previous model, horizontal and vertical stresses increase linearly with depth and horizontal stresses may exhibit an offset at the ground surface. Vertical gradients for σ_h and σ_H are equal and depend on the type of rock under consideration.

If for simplicity we only consider two different lithologies (the central part of the argillite formations and the two limestone formations) this model seems to match the measured stress profile quite well as shown by the linear interpolations of the stress measurements shown on Fig. 3. Due to the uncertainties on the exact value of σ_H, we only use the values of σ_h to calculate the vertical gradients:

$$\alpha_i = \frac{1}{\rho g}\left(\frac{d\sigma_h}{dz}\right)_i . \tag{9}$$

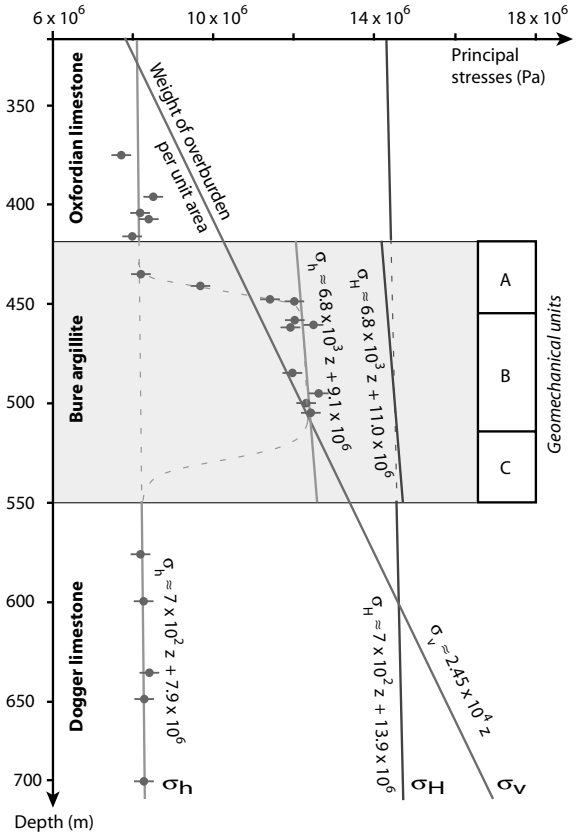

Figure 3. Linear fit to the measured stress profile.

Table 2. Characteristics of the linear fit to the measured stress profile and results of stress inversion according to the fully elastic model.

		Limestone formations (10 measurements of σ_h)	Central part of the argillite formation (8 measurements of σ_h)
Linear regression on the measured stress profiles (least-squares method)	Horizontal stresses gradient $d\sigma_h/dz$ (Pa/m)	0.7×10^3	6.8×10^3
	σ_h extrapolated at $z = 0$ (MPa)	7.9	9.1
	σ_H extrapolated at $z = 0$ (MPa)	13.9	11.0
	Horizontal differential stress $\sigma_H - \sigma_h$	6.0	1.9
Results of stress profile inversion	Initial horizontal to vertical stress ratio $\alpha = (d\sigma_H/dz)/\rho g = (d\sigma_h/dz)/\rho g$	0.029	0.28
	$\varepsilon_H(10^{-4})$	4.0–4.3	19.8–20.4
	$\varepsilon_h(10^{-4})$	1.9–2.2	14.6–15.1

Because only stress magnitudes are modified during horizontal deformation and erosion, gradients do not change with time. Horizontal strains ε_H and ε_h are given by:

$$\begin{cases} \varepsilon_H = \dfrac{1-V_i}{E_i}\left[\sigma_{h,i}^{z=0} + (\kappa_i - \alpha_i)\rho g \Delta z\right] + \dfrac{1}{E_i}(\sigma_H - \sigma_h)_i \\ \varepsilon_h = \dfrac{1-V_i}{E_i}\left[\sigma_{h,i}^{z=0} + (\kappa_i - \alpha_i)\rho g \Delta z\right] + \dfrac{V_i}{E_i}(\sigma_H - \sigma_h)_i \end{cases}. \tag{10}$$

Numerical results are given in Table 2, when calculated with the following rheological parameters deduced from laboratory tests:

$\rho = 2.5\ \mathrm{g\,cm^{-3}} \quad E_L = 35\ \mathrm{GPa} \quad E_A = 4.7\ \mathrm{GPa} \quad \upsilon_L = 0.23 \quad \upsilon_A = 0.3$

The subscripts L and A refer, respectively, to the limestone and argillite formations. Using organic matter transformation ratios, Ménétrier *et al.* (2005) have calculated the maximum burial temperature of the *Bure argillite* formation and have shown that the thickness Δz of the rock 'slice' eroded during the last 65 Myr (since the end of Cretaceous) is about 400 to 600 m in the eastern Paris basin.

Calculated values of ε_h and ε_H are positive so horizontal strains are both shortening strains, which is surprising if considering the present deformation pattern deduced form GPS measurements (Tesauro *et al.* 2005) that suggests a 'strike slip' horizontal strain regime ($\varepsilon_H > 0$ and $\varepsilon_h < 0$). However, it should be pointed out that ε_h and ε_H are not necessarily related only to the Alpine orogeny. They correspond to the total horizontal strains the rock mass has been submitted to since the initial stage defined by eq. (4). On the basis of a very detailed microtectonic to regional-scale tectonic framework analysis, André (2003) concluded that the area under consideration was essentially affected by (i) a N–S shortening during the Pyrenean orogeny (Eocene), (ii) a E–W extension during the Western European rifting stage (Oligocene) and (iii) a NNE–SSW shortening during the Alpine orogeny (Miocene). If the initial stage is supposed to correspond to the stress state prior to any tectonic deformation, the current values of ε_h and ε_H may, in a first approach, partly incorporate these three major tectonic events. However, at the present stage of the analysis, this hypothesis should be considered with caution since other stress-disturbing mechanisms and structural effects may also influence the present stress field. The value of horizontal strains should also be determined by an independent method such as that suggested by Oertel (1983).

The two last lines of Table 2 outline an incompatibility between the calculated horizontal strains in the argillite and limestone formations, which should be equal according to our model. Otherwise there would be a shear zone at the interfaces between the formations. This discrepancy may be ascribed either to the assumptions on which our model is based (e.g. fully homogeneous deformation during horizontal shortening without any buckling, no horizontal displacements during erosion, etc.) or to the rheological properties we used for calculation. In fact, those were determined by mean of laboratory tests lasting several minutes to hours and performed on samples of several centimetres size. However, the model deals with duration of several million of years and large volumes, which implies large-scale effects whose consequences are difficult to evaluate. Moreover, we assumed that argillite behaves elastically whereas complementary laboratory tests have demonstrated its viscoelastic behaviour, as discussed in the next section.

It should be noticed that this model implies the following relation:

$$\varepsilon_H - \varepsilon_h = \frac{1}{2G_A}(\sigma_H - \sigma_h)_A = \frac{1}{2G_L}(\sigma_H - \sigma_h)_L, \tag{11}$$

where G stands for the elastic shear moduli. It expresses the fact that the ratio between the limestone and argillite shear moduli should be equal to the ratio between the horizontal differential stresses within these formations for the inverse problem to have a solution. This constraint is not fulfilled in our case because $G_L/G_A = 15.4/1.8 = 8.5$ while $(\sigma_H - \sigma_h)_L/(\sigma_H - \sigma_h)_A = 6/1.9 = 3.2$. This important point is discussed further in Section 5.1.

4 TAKING INTO ACCOUNT THE VISCOELASTIC RHEOLOGY OF THE ARGILLITE FORMATION

4.1 Laboratory creep and relaxation tests on argillite samples

Numerous laboratory tests have been carried out on the *Bure argillite* in order to quantify its time-dependent behaviour (Boidy 2002; Gasc-Barbier *et al.* 2004; Zhang *et al.* 2004; Zhang & Rothfuchs 2004), namely slow-straining triaxial compression tests, short- and long-duration

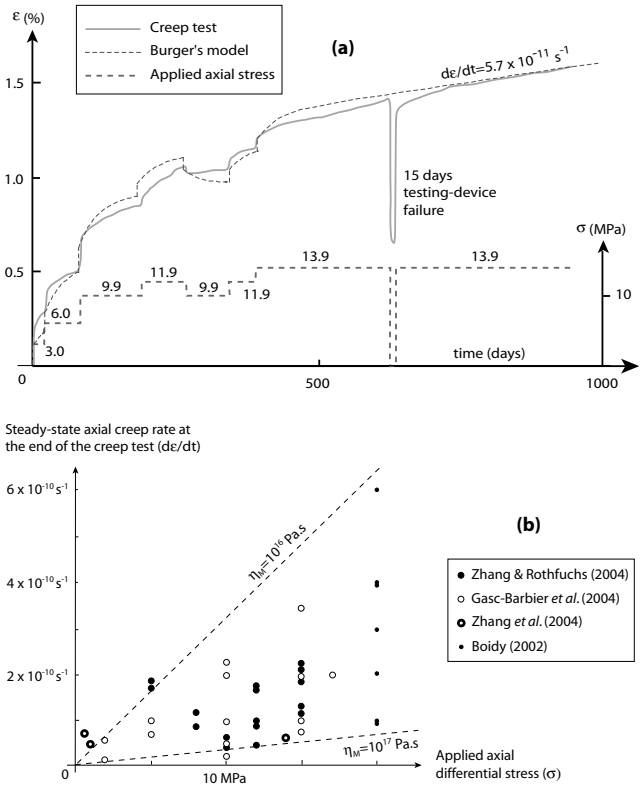

Figure 4. Laboratory creep tests performed on A-type samples of *Bure argillite*. (a) Typical creep curve obtained on an A-type sample (depth 484.2 m in borehole EST205, Zhang *et al.* 2004) and fit of Burger's model ($E_0 = 3$ MPa, $G_K = 0.6$ MPa, $\eta_M = 8 \times 10^{16}$ Pa s, $\tau_K = 30$ days). (b) Compilation of stable deformation rates obtained at the end of creep experiments performed on A-type samples (Gasc-Barbier *et al.* 2004; Zhang & Rothfuchs 2004; Zhang *et al.* 2004).

creep tests (deformation under constant stress, over up to 3 years) and short-duration relaxation tests (stress relief when lateral expansion is prevented, over a few days or weeks).

Typical curves representing axial deformation (ε) versus time (t) during creep tests are presented on Figs 4(a) and 5(a). They are interpreted as a succession of:

(i) An immediate elastic response of the rock sample when axial stress σ is suddenly increased;

(ii) A transient primary creep phase lasting several days or weeks, during which the axial strain rate $d\varepsilon/dt$ rapidly decreases;

(iii) A secondary creep phase essentially depending on the mineralogical and water content of the samples, during which the strain rate seems to reach a constant value (A-type samples, as the one corresponding to Fig. 4a) or decreases slowly until it becomes almost not measurable (B-type samples, as the one corresponding to Fig. 5a).

Final creep rates of all tested A-type samples (samples that seemed to lead to steady-state creep) have been collected and are presented on Fig. 5(b). They seem to increase with applied stress, despite some scattering probably due to slight changes in lithology. The question of existence or absence of a creep-initiation threshold has not been completely elucidated (Gasc-Barbier *et al.* 2004; Zhang & Rothfuchs 2004) but light has been shed on creep deformations for differential stresses as low as 0.73 MPa (with a corresponding deformation rate $d\varepsilon/dt = 6.7\,10^{-11}\,\mathrm{s}^{-1}$).

As regards relaxation tests (Fig. 5c), they did not last long enough to conclude with certainty whether the deviatoric stress would completely relax or not. According to Boidy (2002) it would not and, to the contrary, a permanent stress state with a deviatoric component would be reached. However, this proposition has to be supported by complementary measurements.

4.2 Constitutive equations of Burger's substance

Various creep laws have been proposed to describe the time-dependent behaviour of rocks, some of which rely on simple physical combinations of springs and dash-pots. Among these, Burger's substance is the simplest model that is able to reproduce immediate elastic response as well as primary and secondary creep. In 1-D, it is usually represented as an association of perfectly elastic springs and Newtonian viscous dash-pots gathered in Kelvin and Maxwell cells, as illustrated on Fig. 6(a). Its constitutive equations, relating the axial stress σ and the axial strain ε

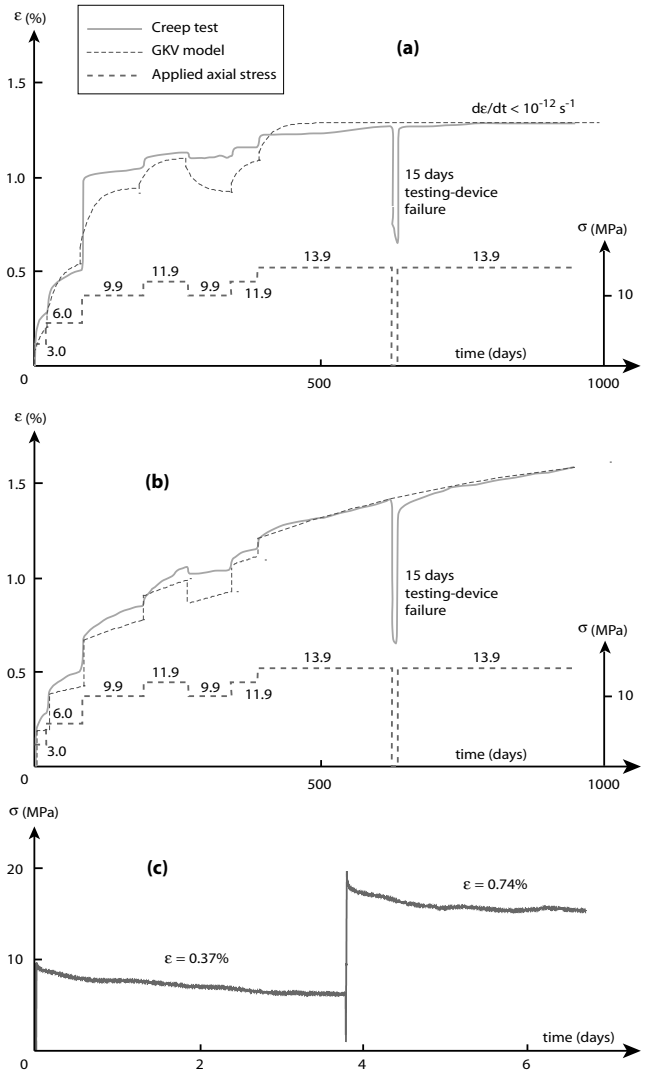

Figure 5. (a) Typical creep curve obtained on B-type samples of *Bure argillite* (depth 434.6 m in borehole EST205, Zhang *et al.* 2004) and fit of a GKV model ($E_0 = 4$ MPa, $G_K = 0.5$ MPa, $\tau_K = 20$ days). (b) Fit of a GKV model to the A-type creep curve presented on Fig. 4(a) ($E_0 = 1.6$ MPa, $G_K = 0.5$ MPa, $\tau_K = 500$ days). (b) Relaxation test performed on a sample of *Bure argillite* (depth 454.6 m in borehole EST205) showing incomplete stress relief (Zhang & Rothfuchs 2004).

(respectively, ε_K and ε_M for the Kelvin and Maxwell cells), are given by:

$$\begin{cases} \eta_K \dfrac{\partial \varepsilon_K}{\partial t} + G_K \varepsilon_K = \sigma \\ \dfrac{\partial \varepsilon_M}{\partial t} = \dfrac{1}{G_M}\dfrac{\partial \sigma}{\partial t} + \dfrac{1}{\eta_M}\sigma \end{cases}, \tag{12}$$

with $\varepsilon = \varepsilon_K + \varepsilon_M$ (Jaeger & Cook 1976, chapter 11, eq. 24).G_K and G_M represent the shear moduli, η_K and η_M the viscosity coefficients.

To obtain the governing equation of Burger's model in 3-D, we follow Jaeger & Cook (1976, section 11.4) in replacing σ and ε in eq. (12), respectively, with the deviatoric stress tensor $\overline{\overline{s}} = \overline{\overline{\sigma}} - \frac{\mathrm{tr}\overline{\overline{\sigma}}}{3}\overline{\overline{1}}$ and with the deviatoric strain tensor $\overline{\overline{e}} = \overline{\overline{\varepsilon}} - \frac{\mathrm{tr}\overline{\overline{\varepsilon}}}{3}\overline{\overline{1}}$ and in multiplying the left-hand terms by a factor 2. Hence:

$$\begin{cases} 2\eta_K \dfrac{\partial \overline{\overline{e_K}}}{\partial t} + 2G_K \overline{\overline{e_K}} = \overline{\overline{s}} \\ \dfrac{\partial \overline{\overline{e_M}}}{\partial t} = \dfrac{1}{2G_M}\dfrac{\partial \overline{\overline{s}}}{\partial t} + \dfrac{1}{2\eta_M}\overline{\overline{s}} \end{cases}, \tag{13}$$

with $\overline{\overline{e}} = \overline{\overline{e_K}} + \overline{\overline{e_M}}$. By combining these equation, the constitutive law for deviatoric behaviour may be written as follows:

$$2\eta_K \frac{\partial^2 \overline{\overline{e}}}{\partial t^2} + 2G_K \frac{\partial \overline{\overline{e}}}{\partial t} = \frac{\eta_K}{G_M}\frac{\partial^2 \overline{\overline{s}}}{\partial t^2} + \left(1 + \frac{\eta_K}{\eta_M} + \frac{G_K}{G_M}\right)\frac{\partial \overline{\overline{s}}}{\partial t} + \frac{G_K}{\eta_M}\overline{\overline{s}}. \tag{14}$$

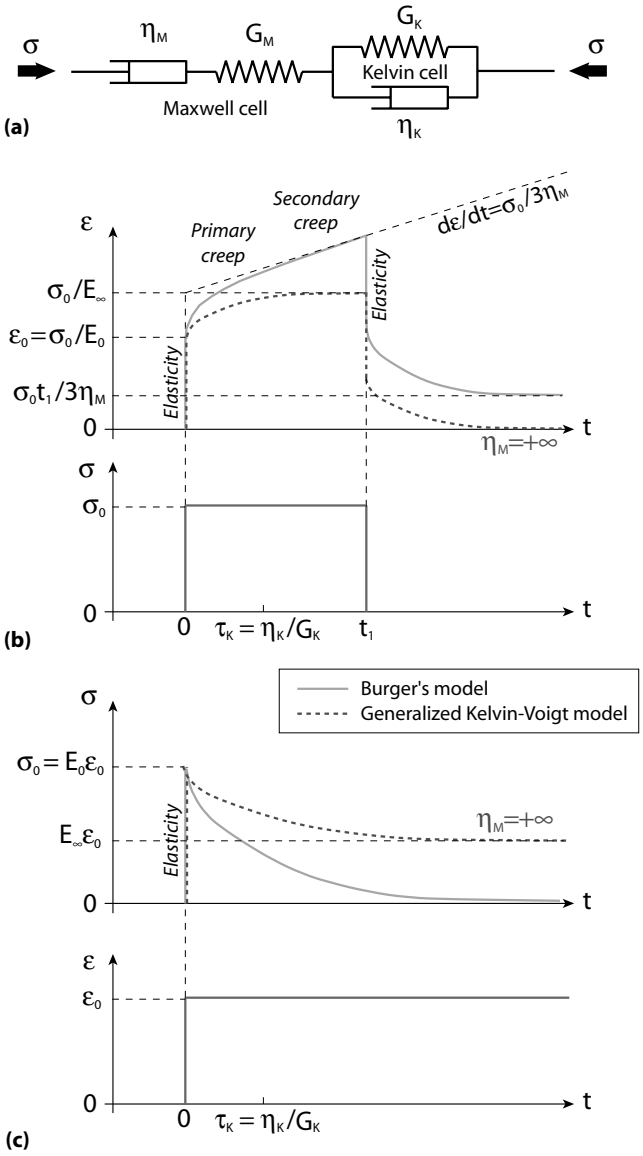

Figure 6. (a) Burger's and GKV models. Theoretical behaviour during uniaxial creep (b) and relaxation (c) tests.

Eq. (14) is not sufficient to completely describe the time-dependent behaviour of Burger's substance and it is necessary to provide also a constitutive law for the bulk behaviour. For simplicity, it is often assumed that the material behaves elastically under hydrostatic compression. Hence:

$$\mathrm{tr}\overline{\overline{\sigma}} = 3K\ \mathrm{tr}\overline{\overline{\varepsilon}}. \tag{15}$$

K stands for the bulk modulus.

The behaviour of Burger's substance during a creep test, when axial stress σ is changed suddenly from 0 to σ_0 and then kept constant, can be computed analytically (see Appendix A). The axial strain ε is given by:

$$\varepsilon(t) = \left[\frac{1}{E_0} + \frac{1}{3G_K}(1 - e^{-t/\tau_K}) + \frac{t}{3\eta_M}\right]\sigma_0, \tag{16}$$

with $E_0 = \frac{3}{\frac{1}{3K}+\frac{1}{G_M}}$. The parameter $\tau_K = \frac{\eta_K}{G_K}$ corresponds to the characteristic timescale necessary to achieve equilibrium within the Kelvin cell. The immediate elastic effect (for $t \approx 0$) is followed by a transient (primary) creep phase with characteristic duration τ_K and, later ($t \gg \tau_K$), by a steady-state (secondary) creep phase (Fig. 6b). The initial elastic behaviour is entirely controlled by the Maxwell-cell spring, whose equivalent Young's modulus is E_0. In the long term, the primary creep may be neglected and the behaviour is the superposition of an immediate elastic response and a steady-state creep at the constant strain rate $d\varepsilon/dt = \sigma_0/3\eta_M$. The final equivalent Young's modulus is:

$$E_\infty = \frac{\varepsilon(t \to +\infty)}{\sigma_0} = \frac{3}{\frac{1}{3K} + \frac{1}{G_M} + \frac{1}{G_K}} = \frac{1}{\frac{1}{E_0} + \frac{1}{3G_K}} < E_0. \tag{17}$$

Table 3. Parameters of Burger's model and of the GKV model for *Bure argillite* inferred from laboratory tests. Parameters of Burger's model are deduced from the A-type creep tests described by Gasc-Barbier *et al.* (2004), Zhang & Rothfuchs (2004) and Zhang *et al.* (2004).

	Immediate elastic response (from Table 1 and laboratory creep test)				Time-dependent behaviour (from laboratory creep tests)					
	E_0 (GPa)	ν_0	G_M (GPa)	K (GPa)	E_∞ (GPa)	ν_∞	G_K (GPa)	η_M (Pa s)	τ_K (Pa s)	η_K (Pa s)
Burger's model	1.6–6.9	0,3 ± 0,05	0.9–2.8	1.7–7.7	1–5	0.35–0.48	0.5–5	10^{16}–10^{17}	Days or weeks	$\sim 10^{15}$
GKV model					Difficult to determine (Section 4.3)			$+\infty$	Difficult to determine (Section 4.3 and 5.2)	

In the same way, equivalent short- and long-term Poisson's ratios may also be defined as $\nu_0 = \frac{1}{2} - \frac{E_0}{6K}$ and $\nu_\infty = \frac{1}{2} - \frac{E_\infty}{6K} > \nu_0$, respectively. As a conclusion, Burger's substance behaves in creep as an elastic body whose Young's modulus and Poisson's ratio change monotonically with time (decrease in Young's modulus and an increase in Poisson's ratio).

To the contrary, during a relaxation test, the axial strain ε is changed suddenly from 0 to ε_0 and then kept constant. The immediate elastic effect is followed by progressive, but complete, vanishing of the axial stress (Fig. 6c) according to the relaxation law:

$$\sigma(t) = \left(\frac{1/\tau_1 - 1/\tau_K}{1/\tau_1 - 1/\tau_2} e^{-t/\tau_1} + \frac{1/\tau_2 - 1/\tau_K}{1/\tau_2 - 1/\tau_1} e^{-t/\tau_2} \right) E_0 \varepsilon_0 \tag{18}$$

(Appendix A). τ_1 and τ_2 stand for two characteristic timescale that may be expressed as functions of the parameters of Burger's substance.

4.3 Is Burger's model adequate for modelling *Bure argillite*?

Boidy (2002) models the mechanical behaviour of the *Bure argillite* with the power law developed by Lemaitre & Chaboche (1996) for metals and determines the corresponding parameters from specific triaxial tests. Here, we investigate the suitability of Burger's model, for explaining the present state of stress. Its much simpler mathematical formulation allows complete analytical calculations.

Among its five parameters (G_M, K, G_K, η_M and η_K), the first two are already known at laboratory scale, from tests summarized in Table 1: $G_M = \frac{E_0}{2(1+\nu_0)}$ and $K = \frac{E_0}{3(1-2\nu_0)}$. The three remaining parameters (G_K, η_M and η_K) may be derived from the creep tests:

(i) The value of E_∞ is derived from the long-term deformation that cannot be attributed to steady-state creep. It leads to an estimation of $G_K = (\frac{3}{E_\infty} - \frac{3}{E_0})^{-1}$ and $\nu_\infty = \frac{1}{2} - \frac{E_\infty}{6K}$.

(ii) The Maxwell-cell viscosity η_M is determined from the steady-state creep rate that is reached after several months of creep (Gasc-Barbier *et al.* 2004; Zhang & Rothfuchs 2004) using the relation: $\eta_M = \frac{\sigma_0}{3(\frac{\partial \varepsilon}{\partial t})_{t \to +\infty}}$ (see Fig. 4b).

(iii) The Kelvin-cell viscosity η_K is estimated on the basis of the transitory creep phase characteristic duration τ_K that seems to be of the order of magnitude of several days or weeks in our case: $\eta_K = \tau_K G_K$.

Numerical values are given in Table 3. An example of fit of Burger's model with a creep test performed on an A-type sample is shown on Fig. 4(a).

Even if Burger's model satisfactorily describes the behaviour of most of the argillite samples under laboratory creep-test conditions, the existence of a steady-state creep phase is not compatible with other data:

(i) First, during creep tests performed on B-type samples the viscous deformation continuously decreases (Fig. 5a).

(ii) Second, during relaxation tests the stress relief does not seem to be complete (Fig. 5c and Boidy 2002), unlike the trend deduced from eq. (18) when $t \to +\infty$.

(iii) Third, in the hypothesis of steady-state creep, the observed horizontal differential stress of 2 MPa in the centre of the argillite formation would lead to a horizontal deformation rate equal to $d\varepsilon/dt = \sigma_0/3\eta_M = 10^{-11}\ \mathrm{s}^{-1}$, in contradiction with the much lower value estimated by Tesauro *et al.* (2005) for this region from GPS monitoring. According to these authors, the deformation rate in the Bure region is bellow the margin of error of the available GPS measurements and at most equal 4 to 7 $10^{-9}\ \mathrm{yr}^{-1}$, that is, 1.4 to 2.2 $\times\ 10^{-16}\ \mathrm{s}^{-1}$.

The first two discrepancies may be attributed to experimental uncertainties or to a lack of control on other parameters (changes in pore pressure, mechanical damaging of the sample during coring, etc.). The last one is much more fundamental, as it raises questions on the space and timescale effects. Actually, it leads to eliminating the effect of the Maxwell-cell dashpot and thus to considering that $\eta_M = +\infty$ (see dotted lines on Figs 6b and c) when considering geological time and spacescales. In this latter case, Burger's model is known as a 'Generalized Kelvin–Voigt' (GKV) model (or standard linear solid) and the creep law becomes:

$$\varepsilon(t) = \left[\frac{1}{E_0} + \frac{1}{3G_K}(1 - e^{-t/\tau_K}) \right] \sigma_0. \tag{19}$$

Thus, when t becomes much greater than τ_K an equilibrium axial strain σ_0/E_∞ is reached, without further creep, which matches the behaviour of B-type samples (dashed line on Fig. 5a). As regards relaxation, according to equation pair (A9), one time constant has to be equal to infinity

(let $\tau_2 = +\infty$) and the other one (τ_1) has to be such that:

$$\frac{1}{\tau_1} = \frac{1}{\tau_K} + \frac{E_0}{3\eta_K} = \frac{1}{\tau_K}\frac{E_0}{E_\infty}. \tag{20}$$

As a consequence, the relaxation law may be written:

$$\sigma(t) = \left[(E_0 - E_\infty)e^{-t/\tau_1} + E_\infty\right]\varepsilon_0, \tag{21}$$

and deviatoric stresses do not relax completely, but stabilize at the value $E_\infty\,\varepsilon_0$.

If we question the adequacy of Burger's substance model, we also have to reconsider our first interpretation of creep tests performed on A-type samples (Fig. 4a). We assumed the primary creep phase has a characteristic duration of several days or weeks (τ_K) and, after that time, creep-rate remains constant. However, actually, we cannot rule out that the primary creep phase has a much longer duration and that we only see part of it. In that case, the creep rate may decrease progressively if the creep test goes on, until the rock reaches a static equilibrium state, as for B-type samples. By comparing Figs 4(a) and 5(b), it seems that the GKV model is also able to reproduce the long-term behaviour of A-type samples. (The quality of the fit seems to be less than previously because there is one more parameter in Burger's model than in the GKV one, that is, one more degree of freedom for the fit.) This implies that identifying true steady-state creep in creep test is difficult and thus, that long-term parameters of Burger's or GKV models can hardly if ever be derived from creep tests, even if they last several years.

One should also notice that, changing from a Burger's to a GKV substance has a major impact on the interpretation of the long-term behaviour of the rock mass. In the long term, in the first case, it behaves like a liquid (deviatoric stresses progressively decrease to zero), whereas in the second case it behaves like a solid (possible permanent deviatoric stresses). In our case, the Burger's model is unrealistic because the argillite exhibits a horizontal differential stress equal to about 2 MPa whereas the loading source (the last tectonic event) has disappeared several million years ago.

4.4 Analytical and numerical calculation of the state of stress in the argillite

In order to verify whether the rheology we suggest for the Bure argillite—namely a GKV model—is compatible with the present state of stress that exists within this formation, we calculate analytically the stress state at the end of the shortening and erosion processes.

Let us assume that the initial state of stress within the argillite is horizontally isotropic and governed by a horizontal to vertical stress ratio α_A (eq. 4). If the duration since the end of the tectonic shortening ($t - t_{\text{tecto}}$, with t being the present time) is small compared to the durations τ_K or τ_1 (actually τ_K and τ_1 are of the same order of magnitude), the stress state after horizontal shortening will be given by the short-term elastic parameters E_0 and ν_0:

$$\begin{cases} \sigma_v = \rho g(z + \Delta z) \\ \sigma_H = \alpha_A \rho g(z + \Delta z) + \dfrac{E_0}{1 - \nu_0^2}(\varepsilon_H + \nu_0 \varepsilon_h) \\ \sigma_h = \alpha_A \rho g(z + \Delta z) + \dfrac{E_0}{1 - \nu_0^2}(\nu_0 \varepsilon_H + \varepsilon_h) \end{cases} \tag{22}$$

However, since the main tectonic deformation took place at least 5×10^6 years ago, it is more realistic to assume that $t - t_{\text{tecto}}$ is large compared to τ_K. Thus, relaxation had plenty of time to take place and the present stress state is given by the long-term parameters E_∞ and ν_∞:

$$\begin{cases} \sigma_v = \rho g(z + \Delta z) \\ \sigma_H = \alpha_A \rho g(z + \Delta z) + \dfrac{E_\infty}{1 - \nu_\infty^2}(\varepsilon_H + \nu_\infty \varepsilon_h) \\ \sigma_h = \alpha_A \rho g(z + \Delta z) + \dfrac{E_\infty}{1 - \nu_\infty^2}(\nu_\infty \varepsilon_H + \varepsilon_h) \end{cases} \tag{23}$$

As regards erosion, the problem is more complicated since this process is still active today. Nevertheless, if we assume that the major part of erosion (erosion of the slice of thickness Δz) took place at time t_{erosion}, we may distinguish between two extreme cases. If $t - t_{\text{erosion}}$ is small compared to τ_K, horizontal stress relaxation has not occurred yet and:

$$\begin{cases} \sigma_v = \rho g z \\ \sigma_H = \alpha_A \rho g(z + \Delta z) + \dfrac{E_\infty}{1 - \nu_\infty^2}(\varepsilon_H + \nu_\infty \varepsilon_h) - \kappa_0 \rho g \Delta z \\ \sigma_h = \alpha_A \rho g(z + \Delta z) + \dfrac{E_\infty}{1 - \nu_\infty^2}(\nu_\infty \varepsilon_H + \varepsilon_h) - \kappa_0 \rho g \Delta z \end{cases} \tag{24}$$

If now, we assume that $t - t_{\text{erosion}}$ is large compared to τ_K, we have:

$$\begin{cases} \sigma_v = \rho g z \\ \sigma_H = \alpha_A \rho g z + \dfrac{E_\infty}{1 - \nu_\infty^2}(\varepsilon_H + \nu_\infty \varepsilon_h) - \kappa_\infty \rho g \Delta z \\ \sigma_h = \alpha_A \rho g z + \dfrac{E_\infty}{1 - \nu_\infty^2}(\nu_\infty \varepsilon_H + \varepsilon_h) - \kappa_\infty \rho g \Delta z \end{cases} \tag{25}$$

In the more general case with only partial stress relaxation, the present stress state may be written as an intermediate state between these two extreme cases. The complete calculation is provided in Appendix B.

4.5 Complete inversion of the stress profile

Similarly to the fully elastic model discussed in Section 3, parameters of the GKV model cannot be determined from laboratory tests only, due to scale effects. We propose hereafter a method for deriving them from natural stress profiles analysis. No matter which of the previous models we decide to use, calculated stresses in the argillite formation always depend linearly on depth (with σ_h and σ_H having the same vertical gradient), as it is the case for the limestone formations that are still supposed to behave elastically (eq. 7). Thus, using the characteristic values of the measured stress profiles given in Table 2, we may calculate the long-term rheological parameters of the limestone (E_L, ν_L) and the argillite (E_∞, ν_∞) formations as well as the total horizontal strains (ε_h and ε_H).

We illustrate this methodology by using the model described by eq. (24), but a similar stress inversion may also be performed using any other model. In our case, the relations to be used to infer the unknowns E_L, E_∞, ν_L, ν_0, ν_∞, ε_H and ε_h are:

$$\begin{cases} (\sigma_H - \sigma_h)_L = \dfrac{E_L}{1+\nu_L}(\varepsilon_H - \varepsilon_h) \\ (\sigma_H - \sigma_h)_A = \dfrac{E_\infty}{1+\nu_\infty}(\varepsilon_H - \varepsilon_h) \\ (\sigma_h^{z=0})_L = \dfrac{E_L}{1-\nu_L^2}(\nu_L\varepsilon_H + \varepsilon_h) + (\alpha_L - \kappa_L)\rho g \Delta z \\ (\sigma_h^{z=0})_A = \dfrac{E_\infty}{1-\nu_\infty^2}(\varepsilon_H + \nu_\infty\varepsilon_h) - (\alpha_A - \kappa_0)\rho g \Delta z \end{cases} \tag{26}$$

Moreover, we have:

$$\alpha_i = \frac{1}{\rho g}\left(\frac{\partial \sigma_h}{\partial z}\right)_i = \frac{1}{\rho g}\left(\frac{\partial \sigma_H}{\partial z}\right)_i . \tag{27}$$

Actually, due to the expression of the set of eq. (26), we cannot calculate separately the Young moduli and the strains. We only have access to their products: $E_L\varepsilon_H, E_L\varepsilon_h, E_\infty\varepsilon_H$ and $E_\infty\varepsilon_h$. Since $E_L\varepsilon_H/E_L\varepsilon_h = E_\infty\varepsilon_H/E_\infty\varepsilon_h$, these quantities represent three independent data. Another three parameters are needed for solving the problem, namely: ν_L, ν_∞ and ν_0. Thus, the global number of model parameters is 6. Since we have only four different equations, there is not one unique solution. However, in practice, solution domains are quite well constrained because of the necessity to also satisfy the following rules:

$$\begin{cases} 0 < \nu_L < 0.5 \\ 0 < \nu_0 < \nu_\infty < 0.5 \end{cases} \tag{28}$$

It may be shown that, for $\Delta z = 500$ m, all solutions are very close to:

$\nu_L = 0.1 \pm 0.05 \qquad \nu_\infty = 0.48 \pm 0.01 \qquad \nu_0 = 0.15 \pm 0.05$

$E_L\varepsilon_H = 1.4\ 10^7$ Pa $\quad E_L\varepsilon_h = 7.4\ 10^6$ Pa $\quad E_\infty\varepsilon_H = 6.0\ 10^6$ Pa $\quad E_\infty\varepsilon_h = 3.2\ 10^6$ Pa

The Young's moduli theoretically remain unknown. However, the absence of folding and the near horizontal bedding show that plastic deformation did not propagate from the orogenic collision zone to the site under study. For the case of the Pyrenean orogeny Lacombe & Mouthereau (1999) demonstrated that it remained localized on some pre-existing faults; we believe the same conclusion is valid for the Alpine orogeny. As a consequence, horizontal strains should not be too high in order to avoid plasticity. If we assume they remained lower than 1 per cent, Young's moduli are of the order of magnitude of 0.5–2 GPa, or more.

The values of the parameters calculated for the limestone formations are commented in Section 5.1. Concerning the *Bure argillite* formation, one may notice that the values of ν_0 and ν_∞ differ from the values obtained during classical laboratory testing (0.3 ± 0.05, see Table 1). This difference is related to the time-dependent behaviour of the hard clays. In fact, it has been shown in Section 4.2 that Burger's substance may be compared to an elastic body whose Poisson's ratio continuously increases with time. That is the reason why the value derived from laboratory tests (corresponding to intermediate timescales) lies between the values derived from stress inversion, respectively, for short ($\nu_0 = 0.15 \pm 0.05$) and for long timescales ($\nu_\infty = 0.48 \pm 0.01$). This is in agreement with the fact that the value for short timescales is close to the value deduced from sonic logging (about 0.2).

At this point, our simple model proved able to reproduce the main features of the present stress state in the limestone–argillite–limestone sequence. However, the assumptions we made regarding the homogeneity of the limestone and argillite formations has not allowed reproducing the stress profiles in all its details. In particular we did not try to restore the progressive increase and decrease of σ_h within the A and C geomechanical units of the argillite formation. These are possibly associated with continuous changes in the clay-minerals content at the interfaces between argillite and limestone formations. However, with the limited number of rheological parameters of our model, the apparently intriguing evolution for σ_h and σ_H has been reproduced.

5 DISCUSSION

5.1 Limestone long-term rheology

The two first equations of eq. (26) may be rewritten as follows:

$$(\sigma_H - \sigma_h)_A = \frac{E_\infty}{1+\nu_\infty}(\varepsilon_H - \varepsilon_h) = \frac{E_\infty}{1+\nu_\infty}\frac{1+\nu_L}{E_L}(\sigma_H - \sigma_h)_L = \frac{E_\infty}{1+\nu_\infty}\frac{1}{2G_L}(\sigma_H - \sigma_h)_L. \tag{29}$$

Thus:

$$G_L = \frac{E_\infty}{2(1+\nu_\infty)}\frac{(\sigma_H - \sigma_h)_L}{(\sigma_H - \sigma_h)_A} < \frac{E_0}{2(1+\nu_0)}\frac{(\sigma_H - \sigma_h)_L}{(\sigma_H - \sigma_h)_A} = G_M\frac{(\sigma_H - \sigma_h)_L}{(\sigma_H - \sigma_h)_A} \simeq 3.2G_M. \tag{30}$$

This condition is similar to the one we formulated for the fully elastic model (eq. 11). As said previously, it is not compatible with the results of laboratory tests, which yielded $G_L \approx 15.4$ GPa and $G_M \approx 1.8$ GPa. It means that the overall deformability of the limestone formation is greater—compared to the overall deformability of the argillite formation—at the timescale corresponding to the setting up of natural stresses than at the timescale of laboratory tests.

Actually, if we also take into account dynamic measurements resulting from acoustic borehole logging, we should consider three different timescales: the very short one corresponding to strain wave propagation (less than one second), the intermediate one corresponding to laboratory tests (about several minutes or hours) and the very long one corresponding to the setting up of the present stress state (about hundreds of thousands or million years). The corresponding ratios G_L/G_M (*Dogger limestone* formation compared to the *Bure argillite* one) are, respectively: $17.7/8.7 = 2.0$, $15.4/1.8 = 8.5$ (Table 1) and 3.2. The difference between the first and the second ratio may be explained by the decrease in the stiffness of argillite due to viscous deformation showing up during classical laboratory tests. The difference between the second and the third ratios may be explained by time-dependent deformations of the limestone that only take place over long timescales and cannot be highlighted by laboratory tests.

We propose to explain this higher relative deformability of the limestone formation by a mechanism of pressure solution, that is, of chemical dissolution of calcite minerals under applied stress. Pressure solution is known to be one of the most important mechanisms of rock deformation in the upper crust from 0 to 10–15 km depth (Ramsay 1967; Kerrich 1978; Rutter 1983; Wheeler 1992). It consists of a slow, aseismic, compaction whereby stress enhancement of chemical potential at the contact sites of mineral grains results in local supersaturation of the adjacent fluid, diffusion of the solutes out of the high concentration areas, and precipitation of the material on the grain faces with smaller chemical potential (Zubtsov *et al.* 2005).

The existence of pressure solution in the Bure argillite has already been investigated by mean of indenter tests. No significant evidence of this mechanism was found in these rocks (Gratier *et al.* 2004). On the contrary the large number of both horizontal and vertical stylolites observed on outcrops of the *Dogger* and *Oxfordian limestone* formations (André 2003) is a demonstration that pressure solution took place in these rocks.

The governing law of pressure solution mechanisms is very complex, as it implies simultaneously dissolution, diffusion and precipitation of the material. It is presently difficult to quantify precisely the amount of deformation this phenomenon may be responsible for, particularly since it is not easily reproduced experimentally. However, based on the analytical microscopic approach (at grain-to-grain contact scale) developed by Weyl (1959), Rutter (1976), Raj (1982), Dewers & Ortoleva (1990), Mullis (1991) and Renard *et al.* (1999) it is thought that mechanical effects of pressure solution may be macroscopically similar to those of creep (Angevine & Turcotte 1983; Schneider *et al.* 1996; Revil 2001). For that reason, we assume that pressure solution is characterized by a timescale $\tau_{\rm ps}$ which represents the time necessary to induce a significant part of the final deformation. As the long-term response of the limestone formation to horizontal shortening involves pressure solution, this phenomenon had time to take place between the time of maximum tectonic deformation and present. Therefore, $\tau_{\rm ps}$ should be small in comparison to $(t - t_{\rm tecto})$.

Further work presented in another paper (Gunzburger 2006) leads to better characterization of pressure solution in calcium-carbonated rocks and to formulation of a macroscopic creep law taking it into account. It also provides an expression for $\tau_{\rm ps}$ that indeed appears to be compatible with the previous requirement. Moreover, it shows that deformation by pressure solution does not imply any Poisson's effect so that, as pressure solution progresses, the equivalent macroscopic Poisson's ratio seems to be lower and lower, contrary to what happens with the argillite. This is in good agreement with the very low Poisson's ratio that has been deduced from stress profile inversion. It expresses the fact that, over long timescale, limestone may be strained in one direction without any major deformation in perpendicular directions. (If limestone were also modelled with a GKV substance, viscoelastic deformation would increase the minimum stress even within it, as in the argillite, which is not the case.)

5.2 Initial horizontal-to-vertical stress ratios

Because the two stress-disturbance mechanisms we considered in our model (erosion and horizontal straining) do not affect vertical gradients of principal stresses, the value of α (initial horizontal-to-vertical stress ratio) is equal to the present ratio between horizontal and vertical stress gradients (eq. 27). For simplicity, we have assumed that these gradients are constant within the two limestone formations and within the central part of the argillite formation with, respective, values of 0.029 and 0.28 for α. These values are low and imply that, in the initial state (as defined by eq. 4), horizontal stresses were less than hydrostatic pressure, which may be disconcerting. To avoid such a situation, we

should have:

$$\alpha\rho g(z + \Delta z) \geq \rho_w g(z + \Delta z). \tag{31}$$

Thus $\alpha \geq \rho_w/\rho \approx 0.4$. It is not the case here, especially within the limestone formations. This result can be explained by various reasons.

First, the initial stress state we defined may be too simple and consequently unable to fully reproduce the true initial state. In particular, because the vertical stress is entirely given by the bulk density of the material, the initial stress state is only defined by one parameter α (per homogenous horizontal rock layer), which may be insufficient. We may consider an initial stress state including two unknown parameters α and β per layer, as follows:

$$\begin{cases} \sigma_v = \rho g\,(z + \Delta z) \\ \sigma_H = \sigma_h = \alpha\rho g\,(z + \Delta z) + \beta \end{cases} \tag{32}$$

However, in that case, other relations between rheological properties and stresses are required so that the values of α and β can be solved.

It may be more appropriate not to consider only two different rock layers (argillite and limestone) as we did, because even small changes in rheological properties with depth may implicate changes in α. In that case, eq. (27) we used to determine α should not be used anymore. In fact, even if the vertical gradient of the vertical stress can still be defined (because the vertical stress evolves continuously with depth), the vertical gradient of horizontal stresses is meaningless because the latter may display a step-by-step variation with depth. Such a difference in α probably exists between the two limestone units, so we may have integrated together stress measurements that should be treated separately. Two values of α (one for the *Dogger limestone* formation and one for *Oxfordian* one) may be required. Moreover the lower part of the *Oxfordian limestone* formation may be too heterogeneous for one simple value of α to be calculated with the available stress measurements.

The low value of α for the *Bure argillite* formation may be explained by the margin of error on the estimation of σ_h ($\pm$0.25 MPa according to Wileveau *et al.* 2006) and σ_H, and its true value may be slightly different (and larger than 0.4). However, it may be difficult to resolve it more precisely, given that the stress measurement campaign that has been performed at the Bure URL is one of the most comprehensive (in terms of number of measurements per unit depth). The corresponding uncertainty is, therefore, partly an intrinsic one.

This explanation is not valid for the low value of α within the *Dogger limestone* formation because the measurements clearly show that the value of σ_h remains almost the same over a depth interval of about 125 m. Such a very low vertical gradient has rarely, if ever, been described until now. It demonstrates that the magnitude of horizontal stresses is not necessarily controlled by gravity but may imply other processes that progressively modify the vertical gradients. We believe that pressure solution creep may be one of them. Other mechanisms may also be invoked, such as a temporary over-pressuring of the *Oxfordian limestone* formation due to the less permeable overlying *Bure argillite*. Such a mechanism has been evoked by Evans *et al.* (1989), but its effect has not been evaluated quantitatively until now.

5.3 Characteristic timescales

The stress profile inversion we performed allowed us to obtain values for the immediate and long-term stress–strain ratios (ν_L, ν_∞, ν_0, E_L and E_∞) but it does not give any information about the characteristic timescale τ_K and $\tau_{\rm ps}$. This is because we have considered a simplistic case in which viscous-type response of the rock-mass either had plenty of time to develop (elapsed time much larger than the characteristic duration of the involved process) or did not occur at all (elapsed time much shorter than the characteristic duration).

As regards, for example, horizontal stress relief after erosion, we assumed that erosion took place recently enough for the stress relief not to be completed. In that case, part of the horizontal 'over-stresses' associated with the slice of overburden (through Poisson's effect) before its removal are still present after erosion: they are temporarily 'locked-in'. The theoretical evolution of horizontal stresses after erosion may be calculated analytically (Appendix B).

If we return to the model we used for inversion (eq. 24), it may be seen that it corresponds to a case where $t - t_{\rm tecto} \gg \tau_K \gg t - t_{\rm erosion}$ and $t - t_{\rm tecto} \gg \tau_{\rm ps}$. To get a more precise estimation of τ_K and $\tau_{\rm ps}$, it is necessary to quantify the intensity, duration and age of both the horizontal shortening and erosion episodes.

6 CONCLUSIONS

A very comprehensive investigation program has been performed by ANDRA in relation to the development of the Bure Underground Research Laboratory, designed for investigating *in situ* the feasibility of developing a permanent nuclear waste repository. In particular, a complete and detailed estimation of the present state of stress within the local limestone–clay–limestone sequence encountered within the 700 to 350 m depth interval has been obtained.

Such a well-constrained stress profile contains a great amount of information that may be taken advantage of for investigating the rheology of this sedimentary rock mass at geological timescale. An inverse problem approach has been proposed, which involves relations between the measured stress profile and the various parameters that characterize the appropriate stress–strain relationships. A simple viscoelastic model that involves only five parameters has been found sufficient for explaining the main features of the stress field vertical variations.

When compared with argillite, limestone formations appear to be more deformable over long timescales than predicted by laboratory tests. They also exhibit lower Poisson's ratio. This demonstrates that the limestone formations are the site of long-term, slow-rate, deformation processes that we propose to link to pressure solution.

ACKNOWLEDGMENTS

The authors are indebted to ANDRA who sponsored this study, and especially to Patrick Lebon and Yannick Wileveau who took part in this work.

REFERENCES

Amadei, B. & Stephansson, O., 1997, *Rock Stress and its Measurement*, Chapmann & Hall, London.

Amadei, B., Swolfs, H.S. & Savage, W.Z., 1988. Gravity-induced stresses in stratified rock masses, *Rock Mech.,* **21,** 6–20.

ANDRA (Agence Nationale pour la Gestion des Déchets Radioactifs), 2005. *Dossier 2005, ANDRA research on the geological disposal of high-level long-lived radioactive waste—results and perspectives*, Report submitted to the French government.

André, G., 2003. Caractérisation des déformations méso-cénozoıques et des circulations de fluides dans l'Est du Bassin de Paris, *PhD thesis*, Université Henri Poincaré, Nancy, France.

Angevine, C.L. & Turcotte, D.L., 1983. Porosity reduction by pressure solution: a theoretical model for quartz arenites, *Geol. Soc. Amer. Bull.,* **94,** 1129–1134.

Boidy, E., 2002. Modélisation numérique du comportement différé des cavités souterraines, *PhD thesis*, Université Joseph-Fourrier, Grenoble, France.

Cornet, F.H., 1993. The HTPF and integrated stress determination methods, in *Comprehensive Rock Engineering*,Vol. 3, pp. 413–432, ed. Hudson, J., Pergammon Pres, Oxford.

Cornet, F.H. & Burlet, D., 1992. Stress field determinations in France by hydraulic tests in boreholes, *J. geophys. Res.,* **97**(B8), 11 289–11 849.

Dewers, T. & Ortoleva, P., 1990. A coupled reaction/transport/mechanical model for intergranular pressure solution, stylolites, and differential compaction and cementation in clean sandstones, *Geochim. Cosmochim. Acta,* **54,** 1609–1625.

Evans, K.F., Oertel, G. & Engelder, T., 1989. Appalachian stress study: 2. Analysis of Devonian shale core: Some implications for the nature of contemporary stress variations and Alleghanian deformation in Devonian rocks, *J. geophys. Res.,* **94**(B6), 7155–7170.

Gasc-Barbier, M., Chanchole, S. & Bérest, P., 2004. Creep behavior of Bure clayey rock, *Applied Clay Science,* **26,** 449–458.

Gratier, J.-P., Jenatton, L., Tisserand, D. & Guiguet, R., 2004. Indenter studies of the swelling, creep and pressure solution of Bure argillite, *Applied Clay Science,* **26,** 459–472.

Goodman, R.E., 1989. *Introduction to Rock Mechanics*, 2nd edn, John Wiley & Sons, New York.

Gunzburger, Y., 2006. A macroscopic creep law for pervasive pressure solution, Application to limestone long-term deformation, *Geophys. J. Int.*, submitted.

Haimson, B.C., 1993. The hydraulic fracturing method of stress measurement: theory and practice, in *Comprehensive Rock Engineering*,Vol. 3, pp. 395–412, ed. Hudson, J., Pergammon Press, Oxford.

Jaeger, J.C. & Cook N.C.W., 1976. *Fundamentals of Rock Mechanics*, Chapman & Hall, London.

Kerrich, R.K., 1978. An historical review and synthesis of research on pressure solution, *Zentralblatt für Geologie und Paläontologie,* **5/6,** 512–550.

Lacombe, O. & Mouthereau, F., 1999. Qu'est-ce que le front des orogènes? L'exemple de l'orogène pyrénéen (What is the real front of orogens? The Pyrenean orogen as a case study), *C. R. Acad. Sci. Paris, Earth & Planetary Sciences,* **329,** 889–896.

Lemaıtre, J. & Chaboche, J.-L., 1996. *Mécanique des matériaux solides*, Dunod, Paris.

McGarr, A., 1988. On the state of lithospheric stress in the absence of applied tectonic forces, *J. geophys. Res.,* **93**(B11), 13 609–13 617.

Ménétrier, C., Elie, M., Martinez, L., Le Solleuz, A., Disnar, J.-R., Robin, C., Guillocheau, F. & Rigollet, C. 2005. Estimation de la température maximale d'enfouissement du Toarcien et du Callovo-Oxfordien au centre du bassin de Paris par les marqueurs organiques, *C. R. Geosci.,* **337**(15), 1323–1330.

Müller, B., Zoback, M.L., Fuchs, K. *et al.,* 1992. Regional patterns of tectonic stress in Europe, *J. geophys. Res.,* **97**(B8), 11 783–11 803.

Mullis, M., 1991. The role of silica precipitation kinetics in determining the rate of quartz pressure solution, *J. geophys. Res.,* **96**(B6), 10 007–10 013.

Oertel, G., 1983. The relationship of strain and preferred orientation of phyllosilicate grains in rock—A review, *Tectonophys.,* **100,** 413–447.

Raj, R., 1982. Creep in polycrystalline aggregates by matter transport through a liquid phase, *J. geophys. Res.,* **87**(B6), 4731–4739.

Ramsay, J.R., 1967. *Folding and Fracturing of Rocks*, McGraw-Hill, London.

Renard, F., Park, A., Ortoleva, P. & Gratier, J.-P., 1999. An integrated model for transitional pressure solution in sandstones, *Tectonophysics,* **312,** 97–115.

Renard, F., Schmittbuhl, J., Gratier, J.-P., Meakin, P. & Merino, E., 2004. Three-dimensional roughness of stylolites in limestones, *J. geophys. Res.,* **109,** B03209.

Revil, F., 2001. Pervasive pressure solution transfer in quartz sand, *J. geophys. Res.,* **106**(B5), 8665–8686.

Röckel, T. & Lempp, C., 2003. Der Spannungszustand im Norddeutschem Becken, *Erdöl, Erdgas, Kohle,* **119,** 73–80.

Rutter, E.H., 1976. The kinetics of rock deformation by pressure solution, *Phil. Trans. R. Soc. London,* **283,** 203–219.

Rutter, E.H., 1983. Pressure solution in nature, theory and experiment, *J. geol. Soc. Lond.,* **140,** 725–740.

Savage, W.Z., Swolfs, H.S. & Amadei B., 1992. On the state of stress in the near-surface of the Earth crust, *Pageoph,* **138**(2), 207–228.

Schneider, F., Potdevin, J.L., Wolf, S. & Faille, I., 1996. Mechanical and chemical compaction model for sedimentary basin simulators, *Tectonophysics,* **263,** 307–317.

Stephansson, O., 1983. Rock Stress Measurement by Sleeve Fracturing, in *Proceedings of 5th Congress on Rock Mechanics, Melbourne*, vol. F, 129–138, Australian Geomechanics Society.

Tesauro, M., Hollenstein, C., Egli, R., Geiger, A. & Kahle, H.-G., 2005. Continuous GPS and broad scale deformation across the Rhine Graben and the Alps, *Int. J. Earth Sci.,* **94,** 525–537.

Turcotte, D.L. & Schubert G., 2002. *Geodynamics*, 2nd edn, Cambridge University Press, Cambridge, UK.

Warpinski, N.R. & Teufel, L.W., 1989. In-situ stresses in low-permeability, non-marine rocks, *J. Petrol. Tech.,* **41,** 405–414.

Warpinski, N.R. & Teufel, L.W., 1991. In-situ stress measurements at Rainier Mesa, Nevada Test Site–Influence of topography and lithology on the stress state in tuff, *Int. J. Rock. Mech. Min. Sci.,* **28,** 143–161.

Weyl, P.K., 1959. Pressure solution and the force of crystallisation–a phenomenological theory, *J. geophys. Res.,* **61**(11), 2001–2025.

Wheeler, J., 1992. Importance of pressure solution and Coble creep in the deformation of polymineralics rocks, *J. geophys. Res.,* **97**(B4), 4579–4586.

Wileveau, Y., Cornet, F.H., Desroches, J. & Blumling, P., 2006. Complete in situ stress determination at the Bure laboratory site, *Physics and Chemistry of the Earth,* in press.

World stress map. Available online at: www-wsm.physik.uni-karlsruhe.de/

Zhang, C. & Rothfuchs, T., 2004. Experimental study of the hydro-mechanical behaviour of the Callovo-Oxfordian argillite, *Applied Clay Science,* **26,** 325–336.

Zhang, C.-L., Rothfuchs, T., Moog, H., Dittrich, J. & Müller, J. 2004. *Experiments and modelling of thermo-hydro-mechanical and geochemical behaviour of the Callovo-Oxfordian argillite and the Opalinus clay*, GRS-202 report, ISBN 3-931995-69-0.

Zoback, M.D., Barton, C.A., Brudy, M., Castillo, D.A., Finkbeiner, T., Grollimund, B.R., Moos, D.B. & Peska, P. 2003. Determination of stress orientation and magnitude in deep wells, *Int. J. Rock Mech. Min. Sci.,* **40,** 1049–1076.

Zubtsov, S., Renard, F., Gratier, J.-P., Dysthe, D.K. & Traskine, V.Y., 2005. Single contacts pressure solution creep on calcite monocristals, in *Deformation Mechanisms, Rheology and Tectonic: Current States and Future Perspectives*,Vol. 243, pp. 81–95, eds Gapais, D., Brun, J.-P. & Cobbold, P., J. Geol. Soc. Lond., spec. publ.

APPENDIX A: BEHAVIOUR OF BURGER'S SUBSTANCE DURING UNIAXIAL CREEP AND RELAXATION TESTS

Let σ and ε stand for the axial stress and the axial strain during a uniaxial creep or relaxation tests (with no confining pressure) performed on Burger's substance. Then, the axial deviatoric stress and the axial deviatoric strain are given by:

$$s = \sigma - \frac{\mathrm{tr}\overline{\overline{\sigma}}}{3} = \frac{2}{3}\sigma, \tag{A1}$$

$$e = \varepsilon - \frac{\mathrm{tr}\overline{\overline{\varepsilon}}}{3} = \varepsilon - \frac{\mathrm{tr}\overline{\overline{\sigma}}}{9K} = \varepsilon - \frac{\sigma}{9K}. \tag{A2}$$

By expressing eq. (14) along the axis of compression we obtain the following differential equation that describes the behaviour of Burger's substance:

$$E_0\left(\frac{\partial^2\varepsilon}{\partial t^2} + \frac{1}{\tau_K}\frac{\partial\varepsilon}{\partial t}\right) = \frac{\partial^2\sigma}{\partial t^2} + \left[\frac{1}{\tau_K} + E_0\left(\frac{1}{3\eta_M} + \frac{1}{3\eta_K}\right)\right]\frac{\partial\sigma}{\partial t} + \frac{1}{\tau_K}\frac{E_0}{3\eta_M}\sigma, \tag{A3}$$

with $E_0 = \frac{3}{\frac{1}{3K}+\frac{1}{G_M}}$ and $\tau_K = \frac{\eta_K}{G_K}$. This equation is similar in shape with that provided by Jaeger & Cook (1976, chapter 11, eq. 24) but the coefficients are different due to the fact we started from a real 3-D formulation and not from a simplified 1-D one.

During a creep test, the axial stress is changed suddenly from 0 to σ_0 at time t=0 and then kept constant. Evolution of axial deformation with time can be derived by solving the following equation deduced from A3:

$$\tau_K\frac{\partial^2\varepsilon}{\partial t^2} + \frac{\partial\varepsilon}{\partial t} = \frac{\sigma_0}{3\eta_M}. \tag{A4}$$

With the initial conditions:

$$\begin{cases} \varepsilon(t=0) = \dfrac{\sigma_0}{E_0} = \varepsilon_0 \\ \dfrac{\partial\varepsilon}{\partial t}(t=0) = \left(\dfrac{1}{3\eta_M} + \dfrac{1}{3\eta_K}\right)\sigma_0 \end{cases}, \tag{A5}$$

we obtain:

$$\varepsilon(t) = \left[\frac{1}{E_0} + \frac{1}{3G_K}\left(1 - e^{-t/\tau_K}\right) + \frac{t}{3\eta_M}\right]\sigma_0. \tag{A6}$$

During a relaxation test, the axial strain is changed suddenly from 0 to ε_0 and then kept constant. The axial stress can be computed by solving:

$$\frac{\partial^2\sigma}{\partial t^2} + \left(\frac{1}{\tau_K} + \frac{E_0}{3\eta_M} + \frac{E_0}{3\eta_K}\right)\frac{\partial\sigma}{\partial t} + \frac{1}{\tau_K}\frac{E_0}{3\eta_M}\sigma = E_0\varepsilon_0. \tag{A7}$$

Solutions of this differential equation are of the form:

$$\sigma(t) = (Ae^{-t/\tau_1} + Be^{-t/\tau_2})E_0\varepsilon_0, \tag{A8}$$

where A and B are constants. τ_1 and τ_2 are roots of the following equation pair:

$$\begin{cases} \dfrac{1}{\tau_1}\cdot\dfrac{1}{\tau_2} = \dfrac{1}{\tau_K}\cdot\dfrac{E_0}{3\eta_M} \\ \dfrac{1}{\tau_1} + \dfrac{1}{\tau_2} = \dfrac{1}{\tau_K} + \dfrac{E_0}{3\eta_M} + \dfrac{E_0}{3\eta_K} \end{cases}. \tag{A9}$$

Both of them are real and positive numbers, so that they represent two characteristic timescales. They are related to $E_0/3\eta_M$ and $E_0/3\eta_K$ that correspond, respectively, to the characteristic time to achieve equilibrium within the Maxwell cell and for energy exchange between the Maxwell spring and the Kelvin dashpot. With the initial conditions:

$$\begin{cases} \sigma\,(t=0) = E_0\varepsilon_0 = \sigma_0 \\ \dfrac{\partial\sigma}{\partial t}\,(t=0) = \left(\dfrac{1}{3\eta_M} + \dfrac{1}{3\eta_K}\right)E_0^2\varepsilon_0 \end{cases}, \tag{A10}$$

it can be shown that:

$$\sigma(t) = \left(\frac{1/\tau_1 - 1/\tau_K}{1/\tau_1 - 1/\tau_2}e^{-t/\tau_1} + \frac{1/\tau_2 - 1/\tau_K}{1/\tau_2 - 1/\tau_1}e^{-t/\tau_2}\right)E_0\varepsilon_0. \tag{A11}$$

APPENDIX B: PROGRESSIVE STRESS RELIEF AFTER EROSION IN THE CASE OF A GENERALIZED KEVIN–VOIGT MODEL

The governing equation of the GKV substance can be obtained from that of Burger's substance by setting $\eta_M = +\infty$:

$$2\eta_K \frac{\partial \overline{\overline{e}}}{\partial t} + 2G_K \overline{\overline{e}} = \frac{\eta_K}{G_M} \frac{\partial \overline{\overline{s}}}{\partial t} + \left(1 + \frac{G_K}{G_M}\right) \overline{\overline{s}}. \tag{B1}$$

Let us assume that erosion causes the vertical stress to change with time by an amount $\Delta\sigma_v(t) = \rho g \Delta z(t)$ that depends on the rate at which the thickness of the overburden is decreased. Consequently, an additional vertical deformation $\Delta\varepsilon_v(t)$ occurs (no horizontal deformation is allowed in our model at that stage: $\Delta\varepsilon_H = \Delta\varepsilon_h = 0$) and the horizontal stresses change by an amount $\Delta\sigma_H(t) = \Delta\sigma_h(t)$. It can be shown that:

$$\Delta s_H = \Delta\sigma_H - \frac{2\Delta\sigma_H + \Delta\sigma_v}{3} = \frac{1}{3}\left(\Delta\sigma_H - \Delta\sigma_v\right), \tag{B2}$$

$$\Delta e_H = \Delta\varepsilon_H - \frac{\mathrm{tr}\Delta\overline{\overline{\sigma}}}{9K} = -\frac{1}{9K}\left(2\Delta\sigma_H + \Delta\sigma_v\right). \tag{B3}$$

If eq. (B1) is written along the H axis we obtain:

$$\frac{\partial \Delta\sigma_H}{\partial t} + \frac{3K(G_K + G_M) + 4G_K G_M}{\eta_K(3K + 4G_M)} \Delta\sigma_H = \frac{3K - 2G_M}{3K + 4G_M} \frac{\partial \Delta\sigma_v}{\partial t} + \frac{3K(G_K + G_M) - 2G_K G_M}{\eta_K(3K + 4G_M)} \Delta\sigma_v. \tag{B4}$$

If a slice of overburden with thickness Δz is instantaneously removed at time t_{erosion}, the vertical stress is decreased by the amount $\rho g \Delta z$ and:

$$\frac{\partial \Delta\sigma_H}{\partial t} + \frac{3K(G_K + G_M) + 4G_K G_M}{\eta_K(3K + 4G_M)} \Delta\sigma_H = \frac{3K(G_K + G_M) - 2G_K G_M}{\eta_K(3K + 4G_M)} \rho g \Delta z. \tag{B5}$$

Thus $\Delta\sigma_H(t)$ and $\Delta\sigma_H(t)$ are of the form:

$$\Delta\sigma_H(t) = \Delta\sigma_h(t) = A e^{\frac{t_{\text{erosion}} - t}{\tau_{\text{erosion}}}} + B. \tag{B6}$$

With appropriate boundary conditions, it may then be shown that:

$$\Delta\sigma_H(t) = \Delta\sigma_h(t) = \left[\kappa_\infty + (\kappa_0 - \kappa_\infty) e^{\frac{t_{\text{erosion}} - t}{\tau_{\text{erosion}}}}\right] \rho g \Delta z, \tag{B7}$$

with:

$$\kappa_0 = \frac{\upsilon_0}{1 - \upsilon_0} = \frac{3K - 2G_M}{3K + 4G_M}, \tag{B8}$$

$$\kappa_\infty = \frac{\upsilon_\infty}{1 - \upsilon_\infty} = \frac{3K(G_K + G_M) - 2G_K G_M}{3K(G_K + G_M) + 4G_K G_M}. \tag{B9}$$

The characteristic timescale is given by:

$$\frac{1}{\tau_{\text{erosion}}} = \frac{3K(G_K + G_M) + 4G_K G_M}{\eta_K(3K + 4G_M)} = \frac{1}{\tau_K} \cdot \frac{3K\left(1 + G_M/G_K\right) + 4G_M}{3K + 4G_M}. \tag{B10}$$

By solving the differential eq. (B4), the same calculation may be conducted if erosion is regarded as a continuous process, rather than a step-by-step one.